PAPER

Check for updates

Network-reinforcing HACC-*co*-PAM hydrogel electrolytes for suppressed zinc dendrite growth and high-performance zinc-ion batteries†

Luyuan Yang,‡[a] Chenyuan Xu,‡[a] Lingyu Liu,‡[a] Yunwei Li,‡[b] Zheming Chen,[a] Yue Deng,[a] Jun Zhang,[a] Zheyuan Liu, [ID][a] Yu Chao,*[a] Dewu Lin*[c] and Chengkai Yang [ID] *[a]

Zinc-ion batteries (ZIBs) are regarded as one of the most promising energy storage technologies due to their low cost and high safety. However, their practical applications are severely hindered by uncontrolled zinc dendrite growth and detrimental side reactions. Herein, this study integrates a quaternized chitosan (HACC) network with a polyacrylamide (PAM) network to fabricate a dual-network hydrogel electrolyte (HACC-*co*-PAM). The intermolecular network is formed *via* hydrogen bonds between the $-NH_2$ and the $-OH$ group, as well as coordination bonds between $(CH_3)_3N^+ Cl^-$ and $ZnSO_4$. The covalently crosslinked PAM network serves as the second network. Electrostatic interactions between the functional groups (carbonyl and $-OH$) in HACC-*co*-PAM and Zn^{2+} homogenize the Zn^{2+} flux. The abundant functional groups on HACC-*co*-PAM form an interwoven hydrogen bond network and form strong interactions with water to inhibit side reactions. The growth of Zn dendrites is effectively suppressed. The HACC-*co*-PAM electrolyte exhibits an exceptional ionic conductivity of 16.8 mS cm^{-1} and remarkable plasticity with 590% strain. The symmetric Zn–Zn cell operates stably for 550 hours at 1 mA cm^{-2}, while the Zn–MnO$_2$ cells deliver a specific capacity of 160 mA h g^{-1} after 100 cycles. This work provides valuable insights into the design of advanced hydrogel electrolytes for high-performance ZIBs.

Broader context

The global energy transition demands advanced energy storage systems that harmonize safety, sustainability, and scalability. Zinc-ion batteries (ZIBs), regarded as a promising alternative to lithium-based technologies owing to their inherent safety and cost efficiency, have attracted substantial interest for applications in grid-scale energy storage and flexible electronics. However, their practical implementation is impeded by critical challenges such as uncontrolled zinc dendrite proliferation and interfacial parasitic reactions, which arise from the inability of conventional electrolytes to concurrently achieve ionic conductivity and mechanical stability. These limitations highlight the inadequacy of single-component material designs in resolving complex degradation pathways. In this work, we develop a dual-network hydrogel electrolyte (HACC-*co*-PAM) by integrating a quaternized chitosan (HACC) network with a polyacrylamide (PAM) framework. The design capitalizes on synergistic interactions among hydrogen bonding, ionic coordination, and covalent crosslinking to optimize electrolyte functionality. By effectively suppressing dendrite formation and stabilizing electrochemical interfaces, this innovation establishes a novel strategy for designing durable, high-performance ZIBs.

[a]*College of Materials Science and Engineering, Fuzhou University, Fuzhou, Fujian, 350108, China. E-mail: chengkai_yang@fzu.edu.cn, 596780945@qq.com*

[b]*School of Art, Soochow University, Suzhou, Jiangsu, 215031, China*

[c]*State Key Laboratory of Advanced Waterproof Materials, School of Advanced Materials, Peking University, Shenzhen Graduate School, Shenzhen 518055, China. E-mail: dewulin@pku.edu.cn*

†Electronic supplementary information (ESI) available. See DOI: https://doi.org/10.1039/d5eb00055f

‡These authors have contributed equally to this work.

Introduction

ZIBs have emerged as a promising candidate for large-scale energy storage owing to their inherent advantages of high safety, low production cost, and environmental benignity.[1,2] Nevertheless, the practical deployment of ZIBs faces two critical technical bottlenecks: uncontrolled dendrite growth and parasitic side reactions at the electrode–electrolyte interface.[3] These issues compromise the effective ion transport efficiency and trigger gradual capacity fading, ultimately leading to catastrophic battery failure.[4] To address these challenges, extensive strategies have been explored to protect the zinc anode and

optimize the battery microenvironment, thereby mitigating the detrimental effects of aqueous species. Representative approaches include the use of solid electrolytes,[5,6] zinc anode modification,[7] fabrication of artificial solid electrolyte interphase (SEI) layers,[8] and implementation of gel electrolytes.[9–11] Among these, hydrogel electrolytes have garnered significant attention due to their high ionic conductivity, structural stability, and multifunctionality in regulating ion flux.[12]

In the realm of gel electrolytes, several representative materials have been extensively investigated, including polyacrylamide (PAM)-based hydrogels, polyvinyl alcohol (PVA)-based hydrogels, and biomass-derived hydrogels.[13] These materials have garnered widespread attention in battery energy storage due to their distinct physicochemical properties.[14] Among them, PAM, as a widely utilized water-soluble polymer, exhibits exceptional hydrophilicity owing to its unique molecular architecture composed of abundant acrylamide units linked *via* covalent bonds.[15] More importantly, the negatively charged carbonyl groups on PAM chains can coordinate with Zn^{2+} ions to modulate their distribution, thereby enabling regulated Zn deposition.[16] However, covalently crosslinked PAM hydrogels are prone to structural deformation and mechanical degradation during prolonged cycling, which exacerbates heterogeneous Zn plating/stripping behavior.[17] Therefore, the development of PAM-based hydrogel electrolytes with excellent mechanical strength and interfacial chemistry is crucial for realizing high-performance ZIBs.

Chitosan, a natural polysaccharide, exhibits remarkable biocompatibility, biodegradability, and mucoadhesive properties.[18] As a quintessential derivative of chitosan, quaternized chitosan (HACC) is synthesized by grafting quaternary ammonium groups onto the chitosan backbone,[19] which confers exceptional water solubility across a broad pH range, thereby addressing the poor aqueous solubility of pristine chitosan in neutral or alkaline environments.[20] Owing to its high molecular weight, HACC readily forms robust intramolecular and intermolecular hydrogen bonds, endowing it with the capability to stabilize biomacromolecules.[21] Inspired by its unique physicochemical properties, HACC serves as a network reinforcer in hydrogels. The introduction of hydrogen-bonding interactions through HACC effectively enhances the mechanical integrity of hydrogel architectures.

Herein, we developed a dual-network hydrogel electrolyte (HACC-*co*-PAM) *via* a network-reinforcing strategy, which synergistically stabilizes interfacial chemistry and enables dendrite-free, long-cycle-life ZIBs. PAM chains' carbonyl groups coordinate with Zn^{2+} to modulate their distribution. HACC introduction further modulates Zn nucleation/growth kinetics *via* hydrogen-bonding interactions. The cations on quaternary ammonium salts form ionic interactions with SO_4^{2-}, promoting the dissociation of zinc sulfate and further facilitating the migration of Zn^{2+}. By establishing hydrogen-bonding interactions between HACC and PAM chains, HACC acts as a dynamic network modulator to regulate Zn nucleation/growth kinetics and mitigate Zn corrosion. Notably, the assembled

$Zn–MnO_2$ cells retain a specific discharge capacity of 160 mAh g^{-1} after 100 cycles at 1C, demonstrating exceptional capacity retention. This study proposes a mechanically robust dual-network HACC-*co*-PAM hydrogel electrolyte with tailored interfacial properties, offering a promising pathway toward practical ZIB applications.

Results and discussion

Fig. 1a illustrates the fabrication process of the dual-network HACC-*co*-PAM hydrogel electrolyte, with detailed experimental procedures provided in the ESI.† The HACC-*co*-PAM hydrogel is synthesized through the synergistic interplay of robust covalent crosslinking and ionic interactions. The first network is formed *via* hydrogen bonds between the $-NH_2$ groups of PAM and the $-OH$ groups of HACC, as well as coordination bonds between HACC (Cl^- and $(CH_3)_3N^+$) and $ZnSO_4$. This hierarchical architecture enhances the mechanical robustness of the hydrogel by reinforcing the PAM network. The covalently crosslinked PAM network serves as the second network, imparting flexibility to the hydrogel and preventing dendrite penetration. Furthermore, electrostatic interactions between the functional groups (carbonyl and $-OH$) in HACC-*co*-PAM and Zn^{2+} homogenize the Zn^{2+} flux, effectively suppressing parasitic by-product formation and zinc dendrite growth, thereby enabling uniform Zn deposition. These attributes are indispensable for developing high-performance and stable ZIBs. Upon formation of the HACC-*co*-PAM dual-network hydrogel (Fig. 1b and c), its structural features were analyzed using Fourier-transform infrared (FTIR) spectroscopy. The FTIR spectrum of the PAM hydrogel exhibits a prominent N–H stretching vibration peak at 3214 cm^{-1}, a band at 1094 cm^{-1} associated with the in-plane rocking vibration of $-NH_2$,[22] and a C=O stretching peak at 1687 cm^{-1}. In the HACC-*co*-PAM hydrogel, the shifted N–H absorption peak indicates the formation of intermolecular hydrogen bonds between HACC and PAM chains, which contribute to an increased crosslinking density. The red shift of the C=O peak is attributed to Zn^{2+} coordination, which facilitates regulated Zn deposition (Fig. 1d). These results collectively confirm the successful fabrication of the dual-network HACC-*co*-PAM hydrogel electrolyte.

Ionic conductivity is a critical parameter for hydrogel electrolytes. Fig. 2a displays the Nyquist plots of the pure PAM hydrogel electrolyte and the HACC-*co*-PAM hydrogel electrolyte developed in this study. The intercept on the real axis (Z') corresponds to the bulk resistance (R). The ionic conductivity (σ) was calculated using the formula $\sigma = L/(R \times S)$,[32] where L and S represent the thickness and cross-sectional area of the hydrogel, respectively. The dual-network HACC-*co*-PAM composite hydrogel electrolyte exhibits a significantly enhanced ionic conductivity of 16.8 mS cm^{-1}, far surpassing that of the pure PAM hydrogel (11.7 mS cm^{-1}). Furthermore, tensile strength tests were conducted to evaluate mechanical per-
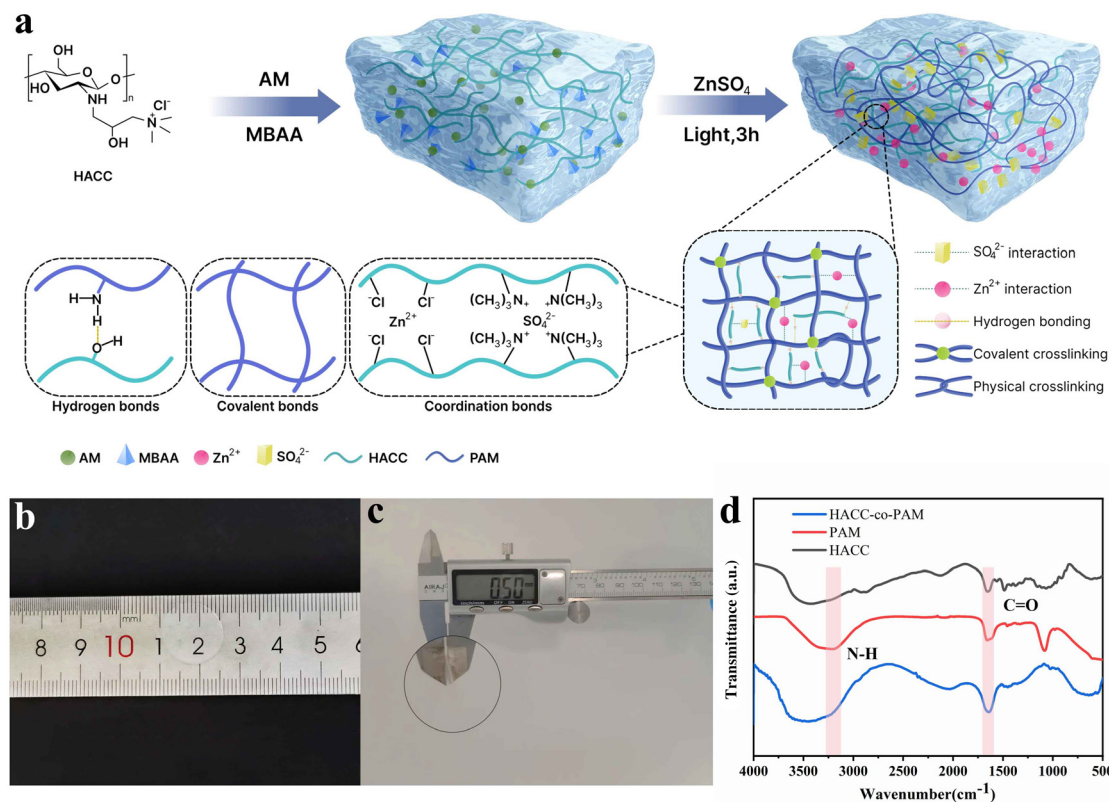
Fig. 1 (a) Preparation of the HACC-*co*-PAM hydrogel. (b) Measurement of the diameter of the prepared HACC-*co*-PAM hydrogel. (c) Measurement of the thickness of the prepared HACC-*co*-PAM hydrogel. (d) FTIR spectra of HACC-*co*-PAM, pure PAM and HACC.
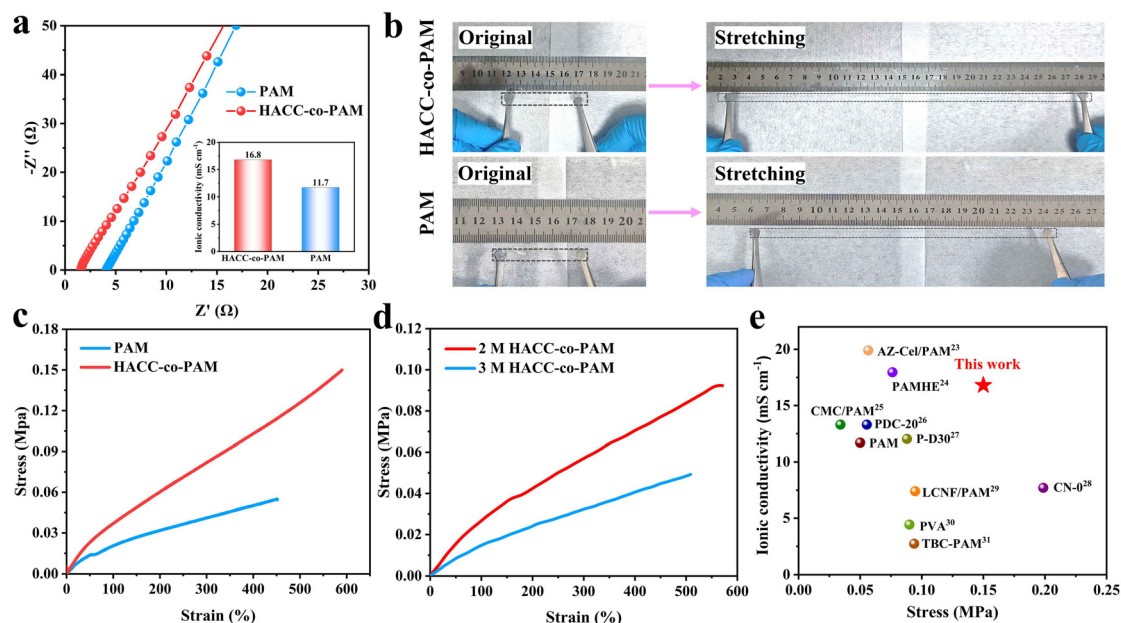
Fig. 2 (a) EIS of the steel−steel cell and ionic conductivity. (b) Digital photos. (c) Stress−strain curves. (d) Tensile stress−strain curves. (e) Comparison of the ionic conductivity and tensile strength with previously reported hydrogels in the literature.[23−31]

formance. Fig. 2b presents a visual demonstration of the HACC-*co*-PAM hydrogel under lateral stretching, highlighting its deformability. The stress–strain curves in Fig. 2c reveal

that the HACC-*co*-PAM hydrogel exhibits a tensile strength of 0.15 MPa, which is 3-fold higher than that of pure PAM (0.05 MPa), while the fracture strain increases from 451% to 590%.

This enhancement is attributed to the intensified non-covalent interactions (*e.g.*, hydrogen bonding and ionic cross-linking) induced by HACC incorporation, which tightens the structural crosslinking and facilitates interpenetration between the dual networks. Regarding the cross-linking changes of hydrogels at higher concentrations of $ZnSO_4$, we synthesized 2 M and 3 M $ZnSO_4$ hydrogels (2 M and 3 M HACC-*co*-PAM hydrogel electrolytes) as shown in Fig. 2d, observing that the stress of hydrogels was 0.09 MPa at 2 M $ZnSO_4$ concentration and 0.05 MPa at 3 M $ZnSO_4$ concentration, which indicates a significant decrease in mechanical properties under the higher concentrations of $ZnSO_4$. This phenomenon was attributed to the fact that the excess salt ions weakened the interaction between the polymer chains and water, which interfered with the formation of crosslinked structures, and ultimately affected the overall stability and mechanical properties of the hydrogels, leading to a decrease in the mechanical properties. Fig. 2e compares the ionic conductivity and tensile strength of various hydrogel electrolytes, which shows that the dual mesh hydrogel electrolyte in this work achieves both excellent ionic conductivity and tensile strength.[23–31] These results collectively show that the dual-network HACC-*co*-PAM hydrogel electrolyte simultaneously achieves exceptional ionic conductivity and mechanical resilience, addressing the longstanding trade-off between ion transport efficiency and structural durability in conventional hydrogel electrolytes.

Linear sweep voltammetry (LSV) tests show that the HACC-*co*-PAM hydrogel achieves an electrochemical stability window of 2.75 V (Fig. 3a), significantly broader than that of the pristine PAM hydrogel (2.63 V) and 1 M $ZnSO_4$ electrolyte (2.51 V). This enhancement is attributed to the denser polymer network in the dual-network HACC-*co*-PAM, which reduces free water activity and thereby expands the electrochemical stability window.[33] The effect of different electrolytes on zinc corrosion was analyzed using the Tafel curve (Fig. 3b), from which it can be seen that the slope of the Tafel curve for the composite hydrogel electrolyte system is smaller than those of the liquid electrolyte and the PAM hydrogel, which indicates that the occurrence of a hydrogen precipitation side reaction on the zinc anode surface can be effectively reduced with the use of the HACC-*co*-PAM composite hydrogel electrolyte. Additionally, electrochemical impedance spectroscopy (EIS) analysis of the Zn–Zn symmetric cell employing the HACC-*co*-PAM hydrogel electrolyte (Fig. 3c) reveals a lower interfacial charge transfer resistance compared to conventional electrolytes, attributable to improved interfacial compatibility, which results from the HACC-*co*-PAM hydrogel electrolyte's ability to effectively suppress dendrite growth.

The initial Zn anode shows a relatively smooth and flat surface (Fig. 3d). Scanning electron microscopy (SEM) images (Fig. 3e) reveal distinct morphological differences in Zn anodes after 20 charge–discharge cycles. The Zn anode cycled in the HACC-*co*-PAM hydrogel electrolyte retains a smooth and compact surface morphology, whereas dendritic growth and surface roughening are observed in the PAM and 1 M $ZnSO_4$ liquid electrolytes. X-ray diffraction (XRD) patterns are
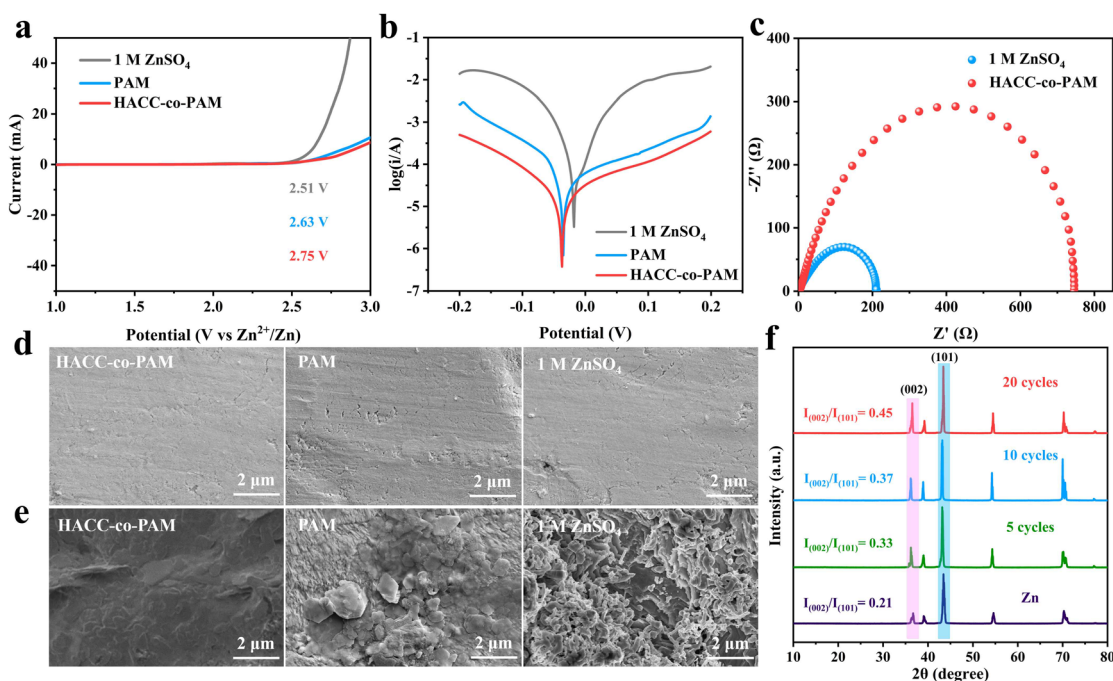
Fig. 3 (a) Oxidation potential curve of the Zn–Ti cell. (b) Tafel curve of the Zn–Zn symmetric cell. (c) EIS of the Zn–Zn symmetric cells. (d) SEM images of the Zn anodes of the Zn–Zn symmetrical cells before the cycles. (e) SEM of the Zn anodes after 20 cycles. (f) XRD of the HACC-*co*-PAM gel electrolyte Zn–Zn cell in different cycles.

employed to investigate the crystal evolution of the Zn anode in the HACC-co-PAM hydrogel electrolyte with different cycles (Fig. 3f). Notably, the peak intensity ratio of (002)/(101) increased significantly from 0.21 to 0.45 after 20 cycles, suggesting that Zn(002) growth was dominant with HACC-co-PAM, resulting in a more uniform electrodeposited Zn surface.[34] The dual-network HACC-co-PAM hydrogel effectively suppresses Zn dendrite formation through a dual mechanism: (i) the negatively charged functional groups on PAM chains electrostatically shield reactive H_2O molecules, minimizing water-induced side reactions, and (ii) coordinated interactions with Zn^{2+} ions homogenize their spatial distribution, enabling epitaxial Zn deposition. These findings robustly demonstrate the superior regulatory capability of the HACC-co-PAM hydrogel electrolyte in controlling Zn nucleation and growth kinetics.

The aforementioned results demonstrate that the incorporation of HACC into the PAM matrix not only enhances mechanical stability under cyclic loading but also significantly improves its capability to regulate uniform Zn deposition. Building on these findings, galvanostatic charge–discharge cycling tests were conducted on Zn–Zn symmetric cells with different electrolytes. At a current density of 1 mA cm^{-2} and an areal capacity of 1 mAh cm^{-2}, the Zn–Zn cell employing the HACC-co-PAM hydrogel electrolyte exhibits an ultralong cycling lifespan of 550 hours with a stable overpotential of about 0.15V (Fig. 4a). These results further underscore the pivotal role of the synergistic interplay between PAM and HACC in enhancing the cycling stability of Zn anodes. It can also be seen from the local magnifications of Fig. 4b–d that the HACC-co-PAM gel electrolyte has good stability. However, the 1 M $ZnSO_4$ liquid electrolyte is polarized after 90 h of cycling under the same test conditions, until it is completely polarized after 132 h of cycling.

We further investigated the long-term electrochemical stability of Zn–Cu asymmetric cells and Zn–Zn symmetric cells employing different electrolytes. Fig. 4e shows the coulombic efficiency plots corresponding to different numbers of cycle turns during charge–discharge cycling for Zn–Cu cells assembled using the HACC-co-PAM composite hydrogel electrolyte with a dual network structure and 1 M $ZnSO_4$ electrolyte. From the figure, it can be clearly observed that the coulombic efficiency of the cell with the 1 M $ZnSO_4$ liquid electrolyte only increased to 94% at the 15th cycle; in contrast, the HACC-co-PAM-based cell achieved a coulombic efficiency of 97% within only 3 cycles. In the subsequent cycle, its coulombic efficiency can be stabilized to maintain a high level of more than 98%. This indicates that the dual network hydrogel electrolyte in this experiment achieves high cycling efficiency. Inspired by the superior mechanical and electrochemical stability of the HACC-co-PAM electrolyte, we systematically evaluated its performance in a Zn–MnO$_2$ cell configuration to assess practical applicability. As shown in Fig. 4f, from the point of view of discharge specific capacity, the starting capacity of the battery using a composite hydrogel electrolyte was about 228.74 larger than that of a liquid electrolyte battery at 212.43. Moreover, the discharge specific capacity of the composite hydrogel electrolyte battery was always maintained above 160, while that of the liquid electrolyte battery was only 51.03 when cycling up to about 47 revolutions; from the point of view of coulombic efficiency, the CE of the battery using the HACC-co-PAM hydrogel electrolyte was always stabilized at more than 98%, while the CE of the battery of using the liquid electrolyte was only about 94%, with a large variation. Therefore, the dual-network HACC-co-PAM hydrogel electrolyte can effectively reduce the occurrence of side reactions in the battery and improve the cycling stability of the battery.
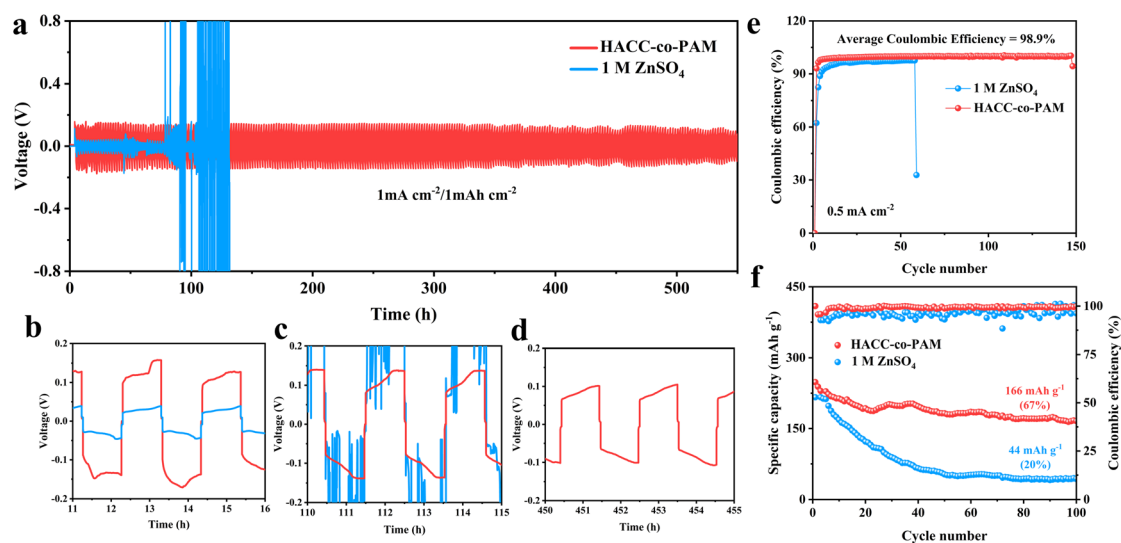

Fig. 4 (a) Cycling performances at 1 mA cm^{-2}/1 mAh cm^{-2}. (b–d) Enlarged images of (a). (e) Zn–Cu cells at 0.5 mA cm^{-2}. (f) Discharge specific capacity and charge/discharge efficiency of the Zn–MnO$_2$ cell.

Conclusion

In summary, this study has successfully developed a dual-network hydrogel electrolyte (HACC-co-PAM) that effectively suppresses dendrite growth and mitigates parasitic side reactions in zinc anodes. This work constructed a dual network structure of PAM and HACC through a hydrogen bonding network, covalent network, and ionic bonding network. The hydrogen bond network enhances the connectivity and inhibits the activity of water. The ionic bond network promotes electrolyte dissociation and Zn^{2+} migration. The hydrogel electrolyte has excellent ionic conductivity (16.8 mS cm^{-1}) and high mechanical strength (590%, 150 kPa). In addition, the symmetric zinc cell containing HACC-co-PAM achieved high cycling stability (550 h at 1 mA cm^{-2}) and the zinc–copper cell achieved high-capacity retention (98% after 150 cycles). The Zn–MnO$_2$ cell retains 67% of its initial capacity (160 mAh g^{-1} after 100 cycles), demonstrating exceptional capacity retention for practical applications. The HACC-co-PAM dual-network gel is a promising strategy that provides a new avenue for large-scale ZIBs applications. Future studies could explore the scalability of HACC-co-PAM hydrogels in flexible battery configurations or under extreme environmental conditions.

Author contributions

Luyuan Yang: conceptualization, formal analysis, investigation, and writing – original draft. Chenyuan Xu: conceptualization and methodology. Lingyu Liu: investigation, data curation, and validation. Yunwei Li: visualization. Zheming Chen: writing – review & editing and supervision. Yue Deng: methodology and software. Jun Zhang: data curation. Zheyuan Liu: supervision. Yu Chao: provision of study materials and supervision. Dewu Lin: supervision and writing – review & editing. Chengkai Yang: conceptualization, supervision and writing – review & editing.

Data availability

The data supporting this article have been included as part of the ESI.†

Conflicts of interest

There are no conflicts to declare.

Acknowledgements

References

1 D. Yang, H. T. Tan, X. H. Rui and Y. Yu, *Electrochem. Energy Rev.*, 2019, **2**, 395–427.

2 L. E. Blanc, D. Kundu and L. F. Nazar, *Joule*, 2020, **4**, 771–799.

3 Q. Zhao, S. Stalin and L. A. Archer, *Joule*, 2021, **5**, 1119–1142.

4 Y. Tan, F. Q. An, Y. C. Liu, S. W. Li, P. G. He, N. Zhang, P. Li and X. H. Qu, *J. Power Sources*, 2021, **492**, 229655.

5 F. L. Li, C. C. Zhou, J. Zhang, Y. T. Gao, Q. Nan, J. M. Luo, Z. M. Xu, Z. J. Zhao, P. Rao, J. Li, Z. Y. Kang, X. D. Shi and X. L. Tian, *Adv. Mater.*, 2024, **36**, 2408213.

6 C. C. Zhou, Z. Y. Wang, Q. Nan, H. Wen, Z. M. Xu, J. Zhang, Z. J. Zhao, J. Li, Z. Y. Xing, P. Rao, Z. Y. Kang, X. D. Shi and X. L. Tian, *Angew. Chem., Int. Ed.*, 2024, **63**, e202412006.

7 N. Maeboonruan, J. Lohitkarn, C. Poochai, A. Tuantranont, P. Limthongkul and C. Sriprachuabwong, *J. Energy Storage*, 2024, **85**, 111063.

8 S. J. Yang, L. L. Zhao, Z. X. Li, P. Wang, Z. L. Liu, J. Shu and T. F. Yi, *Coord. Chem. Rev.*, 2024, **517**, 216044.

9 F. Wan, K. D. Hu, R. Q. Liu, S. D. Zhang, S. F. Li, Y. Lei, D. Yang, C. D. Wang, Y. Y. Xia and W. G. Chen, *Chem. Commun.*, 2024, **60**, 7220–7223.

10 C. C. Zhou, Z. M. Xu, Q. Nan, J. Zhang, Y. T. Gao, F. L. Li, Z. W. Zhao, Z. Y. Xing, J. Li, P. Rao, Z. Y. Kang, X. D. Shi and X. L. Tian, *Adv. Energy Mater.*, 2024, **15**, 2405387.

11 Z. M. Chen, Y. S. Lin, D. H. Shi, K. W. Song, J. Luo, Y. B. Qiu, Z. Y. Liu, Y. Yu and C. K. Yang, *J. Mater. Chem. A*, 2025, **13**, 6709–6718.

12 D. D. Feng, Y. C. Jiao and P. Y. Wu, *Angew. Chem., Int. Ed.*, 2022, **62**, e202215060.

13 Y. F. Li, J. J. Yuan, Y. F. Qiao, H. Xu, Z. H. Zhang, W. Y. Zhang, G. Y. He and H. Q. Chen, *Dalton Trans.*, 2023, **52**, 11780–11796.

14 G. A. Giffin, *J. Mater. Chem. A*, 2016, **4**, 13378–13389.

15 L. T. Ma, S. M. Chen, Z. X. Pei, H. F. Li, Z. F. Wang, Z. X. Liu, Z. J. Tang, J. A. Zapien and C. Y. Zhi, *ACS Nano*, 2018, **12**, 8597–8605.

16 O. Zhanadilov, A. Mentbayeva, Z. Beisbayeva, M. Amze and Z. Bakenov, *Mater. Today: Proc.*, 2022, **49**, 2491–2494.

17 Y. C. Yan, S. D. Duan, B. Liu, S. W. Wu, Y. Alsaid, B. W. Yao, S. Nandi, Y. J. Du, T. W. Wang, Y. Z. Li and X. M. He, *Adv. Mater.*, 2023, **35**, 2211673.

18 W. J. Wang, C. H Xue and X. Z Mao, *Int. J. Biol. Macromol.*, 2020, **164**, 4532–4546.

19 J. F. Niu, J. Wang, K. Qiao, M. Liao, Y. Liu, Y. Ding, H. H. Yao, H. L. Zhang and H. Q. Cao, *Int. J. Biol. Macromol.*, 2024, **262**, 129662.

20 Z. Jin, W. Li, H. W. Cao, X. Zhang, G. Chen, H. Wu, C. Guo, Y. Zhang, H. Kang, Y. F. Wang and K. Zhao, *Chem. Eng. J.*, 2013, **221**, 331–341.

21 L. Wang, Y. Pang, M. H. Xin, M. C. Li, L. L. Shi and Y. F. Mao, *Int. J. Biol. Macromol.*, 2024, **276**, 133777.

22 Q. Liu, Z. L. Yu, Q. N. Zhuang, J. K. Kim, F. Y. Kang and B. Zhang, *Adv. Mater.*, 2023, **35**, 2300498.

23 X. Y. Cheng, T. Li, C. Zhang, Q. Zhang, S. N. Wang, E. Q. Zhu, L. L. Zhang and Z. G. Wang, *J. Colloid Interface Sci.*, 2025, **685**, 948–960.

24 Y. Yang, R. B. Xiao, X. C. Sun, L. H. Lu and Y. Chen, *Mater. Chem. Phys.*, 2022, **287**, 126333.

25 Z. W. Ma, Y. Li, Z. Qu, Z. H. Ma, K. Yang, F. F. Li and B. Xue, *Appl. Clay Sci.*, 2025, **266**, 107691.

26 X. Li, Y. L. Wang, Y. H. Tian, Z. G. Wang, L. L. Zhang and J. X. Ma, *J. Colloid Interface Sci.*, 2024, **670**, 311–322.

27 Y. C. Mao, H. Z. Ren, J. C. Zhang, T. Luo, N. N. Liu, B. Wang, S. R. Le and N. Q. Zhang, *Electrochim. Acta*, 2021, **393**, 139094.

28 T. Y. Zhang, X. H. Shi, Y. Li, S. Sangaraju, F. J. Wang, L. Yang and F. Ran, *Mater. Rep.: Energy*, 2024, **4**, 100272.

29 M. Sun, G. C. Ji and J. P. Zheng, *Chem. Eng. J.*, 2023, **463**, 142535.

30 S. M. Huang, S. G. He, Y. Z. Li, S. F. Wang and X. H. Hou, *Chem. Eng. J.*, 2023, **464**, 142607.

31 S. Chen, J. C. Huang, H. Wang, X. M. Liu, G. H. Gao, X. Liu and Q. Zhang, *Chem. Eng. J.*, 2024, **501**, 157589.

32 J. W. Wang, Y. Huang, B. B. Liu, Z. X. Li, J. Y. Zhang, G. S. Yang, P. Hiralal, S. Y. Jin and H. Zhou, *Energy Storage Mater.*, 2021, **41**, 599–605.

33 W. K. Zeng, S. B. Zhang, J. Q. Lan, Y. Lv, G. Q. Zhu, H. T. Huang, W. Lv and Y. Zhu, *ACS Nano*, 2024, **18**, 26391–26400.

34 J. C. Zhai, W. Z. Zhao, L. Wang, J. B. Shuai, R. W. Chen, W. J. Ge, Y. Zong, G. J. He and X. H. Wang, *Energy Environ. Sci.*, 2025, DOI: **10.1039/d5ee00158g**.